Factors Affecting the Performance of 3D Thermal Mapping for Energy Audits in a District by Using Infrared Thermography (IRT) Mounted on Unmanned Aircraft Systems (UAS)

Y. Hou[a], L. Soibelman[a], R. Volk[b], and M. Chen[a]

[a]Sonny Astani Department of Civil and Environmental Engineering, University of Southern California, USA
[b]Institute for Industrial Production, Karlsruhe Institute of Technology, Germany
E-mail: yuhou@usc.edu, soibelman@usc.edu, rebekka.volk@kit.edu, meidache@usc.edu

Abstract −

Infrared Thermography (IRT) is a widely used non-destructive method for energy audits. However, plenty of research indicates that the performance of passive thermography is influenced by the method of data collection. Unmanned Aircraft Systems (UAS) has been successfully employed for conducting RGB photogrammetry, but the data collected from an infrared thermal camera and an optical camera differ from one another. The infrared Thermal camera usually has a lower display resolution, is more likely influenced by ambient condition, and is limited to the distance between camera and objects. UAS is being utilized for reducing the time and complexity of data collection and for capturing detailed thermal images on large areas like university campuses or entire city districts. Meanwhile, it is important to investigate the impacts of factors such as camera angle, flight patterns, and overlap of pictures when auditing energy of a group of buildings within a district. This paper introduces the preliminary results of a study that tested factors that affect 3D thermal mapping by using a UAS. To measure the performance of mapping, this research compared the quality of rendered images generated from a mapping model constructed by drone acquired data with images acquired directly from a thermal camera. The efficiency of different UAS flying configurations were investigated. The investigation showed that the adjustment of flying configurations can improve the quality of rendered images for energy audits, even though rendered images were not as high-quality as images captured directly from a thermal camera.

Keywords −

Thermal mapping; Unmanned aircraft system (UAS); Flying configurations; Energy audits

1 Introduction

Energy audit has been used to reduce energy loss from buildings and distribution networks for many years. There are plenty of ways in auditing energy loss, including simulation methods, data-driven methods, and Infrared Thermography methods (IRT)[1][2]. Infrared Thermography (IRT), as a non-destructive approach, has been widely utilized for both a quantitative type of approach [3][4] and a qualitative type of approach[5]. However, IRT is influenced by the different approaches for data collection. In general, there are two types of approaches to collecting data for IRT, including Active Thermography and Passive Thermography[6][7][8]. Active Thermography employs an external stimulus to produce an extreme thermal difference (heating or cooling) between the objects and the environment. These approaches can detect hidden defects in detail, but they assume that auditors are fully aware of positions of potential thermal anomalies. Therefore, active approaches cannot be adopted effectively when auditing a whole district. On the contrary, passive thermography does not rely on man-made stimuli. Passive thermography concentrates on observing thermal patterns based on the temperature values and is influenced by weather and thermal emissivity.

Automated fly-past survey is referred as Unmanned Aircraft System (UAS), known as drones, with mounted thermal cameras. Firstly, UAS is flexible to collect thermal information from different angles and different altitudes.[9] Secondly, UAS not only can capture images horizontally, obliquely, and vertically from different angles around a building, but also can fly at a lower altitude and fly through two buildings to capture fine details. Finally, UAS can reduce time and labor. To date, UAS based IRT has been one of the most popular methods used in energy audits. New products, for example, allow the deployment of dual cameras to capture RGB images and thermal images at the same time

from the same angle and altitude. The main issue is that thermal camera's resolution is not as high as optical camera's resolution resulting in a lower quality 3D model generated by photogrammetry mapping.

Although UAS based IRT can reduce the time and complexity of data collection, and capture detailed images throughout a whole district, there remained serval problems in terms of drone flying configurations and efficiency. Additionally, auditing a single building differed from auditing a group of buildings within a district. It was crucial to investigate the impacts of factors such as camera angle, flight patterns, and pictures overlap when auditing energy of a group of buildings within a district. To explore factors affecting the performance of 3D thermal mapping for energy audits by using Infrared Thermography (IRT) mounted on Unmanned Aircraft Systems (UAS), this study proposed a method for testing different combinations of flying configurations and for comparing the results derived from those different combinations. The comparisons were based on quality and efficiency, and different factors' influences were analyzed. The following sections will present the proposed research method, the results, the discussion and conclusions.

2 Research Method

2.1 Architecture of Research Method

This study has three parts, Data Collection[10]; 3D Mapping; and Data Analysis and Comparison. In the first stage, different drone flying configurations in terms of flight patterns (vertical grid, horizontal grid and mesh grid), camera angles (90 and 45 degrees), and the percentage of image overlap (90% and 85%) were tested over a district. In the second stage, the features of every image were detected and used to reconstruct a 3D model. Due to several well-established commercial 3D reconstruction software programs, this process is effortless to implement. In the last stage, all 3D models based on different flying configurations were ranked. The ranking criteria compares the images rendered from 3D models and terrestrial images captured on site at the same time when flying the drone. The rendered images consist of points so relative points can be projected onto captured images. For thermal models and thermal images, points contain the temperature data, and so do the images. Temperature errors can distinguish the performance of different flying configurations. The workflow is shown in Figure 1. Each stage will be introduced in detail in the following paragraphs.
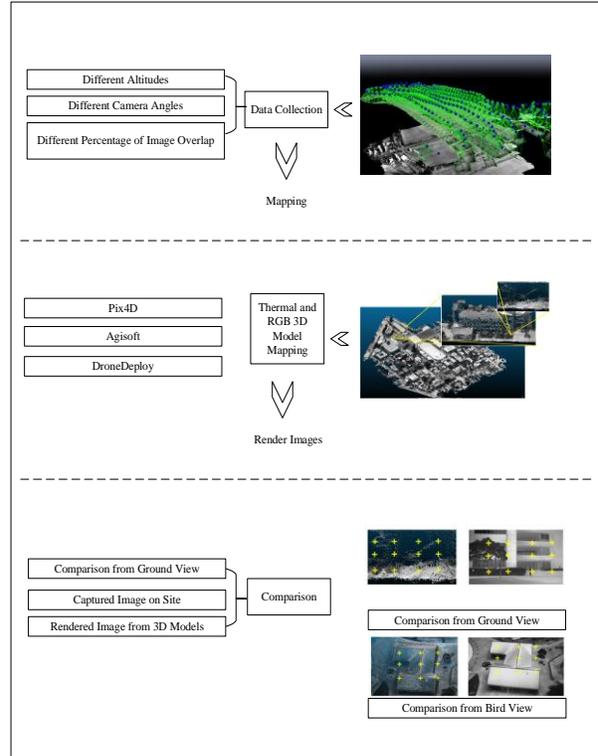

Figure 1. Workflow of research method

2.2 Data Collection

The Unmanned Aircraft System (UAS) used in this study is shown in Figure 2. The UAS consists of three parts: the main body, the data collection system, and the controller. The main body consists of an aircraft and a gimbal. The DJI M600, an industrial level drone, was deployed in this research. Gremsy T3 was the gimbal connecting the camera to the drone. It can horizontally and continuously yaw 360 degrees, has a vertical pitch from positive 90 degrees to negative 135 degrees, and can roll positive and negative 45 degrees. The gimbal can also connect to data collection system. One thermal camera, FLIR DUO Pro R was used in the data collection system. This camera can provide at the same time both a high-resolution featuring thermal image and a high-definition color image in a single integrated package. The data format is known as Radiometric JPEG. This file format contains both thermal and visible data in a single file. The resolutions of visible sensors and thermal sensors are 4000*3000 and 640*512 respectively. An additional benefit of this product is that absolute temperature can be read from its thermal images. The final part of this whole system is the controller. The controller can both remotely operate an aircraft for flight patterns, gimbal for angles, and cameras for data collection.

There are a great number of software programs which can be used for data collection. The available software programs are compared with each other in Table 1. However, not all software can be used to support both a drone system and a camera system. In this study, DIJ GS Pro were used.

2.3 Visible and Thermal 3D Mapping

Due to the overlaps between two pictures, common feature points in different pictures can match with each other. To find common feature points, two widely used methods, Scale-Invariant Feature Transform (SIFT) and Speeded-up Robust Features (SURF) has been introduced. This process is called finding correspondence. To filter incorrectly matched points, Random Sample Consensus (RANSAC) is responsible for removing the outliers. After enough common feature points obtain their matches, the Location Determination Problem (LDP) can be solved and the positions of points can be determined in space. This technique for reconstructing 3D points from two-dimensional image sequences is called Structure from Motion (SfM)[11]. There are plenty of well-established commercial software programs for 3D reconstruction, including Pix4D, Agisoft, and DroneDeply [6] that implement this approach. In this study, Pix4D was used because of its ability to process both RGB and thermal images and to merge RGB and thermal models

(1) Gimbal - Connection to DJI M600; (2) Gimbal - Frame for Camera; (3) FLIR DUO Pro R – Visible Lens Barrel; (4) FLIR DUO Pro R – IR Lens Barrel; (5) FLIR DUO Pro R – Electric Wires; (6) FLIR DUO Pro R – Integration Cable; (7) FLIR DUO Pro R – GPS Antenna Cable; (8) FLIR DUO Pro R – USB Cable.

Figure 2. Cameras setup for the deployed unmanned aircraft system
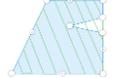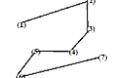
The most significant part in the data collection stage was to test different flying configurations. In this study, different flight patterns (vertical grid, horizontal grid and mesh grid), camera angles (90 and 45degrees), and percentage of image overlap (90% and 85%) were tested.

Table 1. Comparison of data collection software

Designed by	Operated on IOS System	Operated on Android System	Plan Mapping	Circular	Peripherical Mapping	Waypoint Route	360 Degree Panorama
Pix4D Capture	Yes	Yes	Yes	Yes	No	No	No
DIJ GS Pro	Yes	No	Yes	Yes	No	Yes	No
Drone Deploy	Yes	Yes	Yes	No	No	No	No
Drone Harmony	No	Yes	Yes	Yes	Yes	Yes	No
Hangar360	Yes	No	No	No	No	No	Yes
Drone Blocks	Yes	No	Yes (by coding)	Yes (by coding)	No	Yes (by Coding)	Yes (by Coding)

2.4 Data Analysis and Comparison

After images collected through different flying configurations and processed by mapping, different 3D models with different flying configurations were obtained. In this stage, all constructed 3D models can be tested and ranked to determine which UAS flying configurations are the superior ones to audit energy loss.

In this study, data collected with UAS was compared with data captured by terrestrial thermal camera. Temperature values can change over time, however, each flight took less than 15 minutes, a span of time that does not allow temperature values change dramatically. After each flight, cameras have been immediately utilized as a stationary equipment to capture a thermal image close to

a selected building (less then 12m) facing selected façade and windows. Shown in Figure 3 (a), this picture was captured by thermal camera. Meanwhile, this selected viewing position and the same camera parameters were recorded. These setting then can be used to create a virtual camera with the same viewing position in a given 3D mapping model related to the flight to render an image from the model. Shown in Figure 3 (b), this is a rendered image from the thermal model. In order to measure the performance of mapping, quality of rendered images generated from a 3D mapping model, and captured images from a thermal camera were compared. Every point in (b) had color information representing temperature values. The criterion of comparison was to calculate the differences and errors between points in rendered images, illustrated by yellow crosses in (b), and related pixel in captured images, illustrated by yellow crosses in (a).
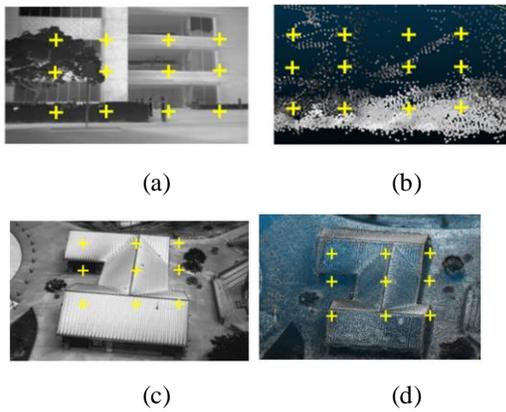

Figure 3. Cameras setup for unmanned aircraft system

One case of comparison was facing façade and windows shown in Figure 3 between (a) and (b). Another case was facing the roof system. In the second case, capturing extra images on site were not necessary. The images that were captured from drone view could be directly employed, shown in Figure 3 is a captured thermal image (c) and a rendered thermal image (d). The same comparison was also conducted for the second case.

To calculate the differences and errors between two images, two mathematical approaches were used being Mean Squared Error (MSE) and Structural Similarity Measure (SSM). Shown in equation (1) and equation (2).

$$MSE = \frac{1}{mn}\sum_{i=0}^{m-1}\sum_{j=0}^{n-1}[I(i,j) - K(i,j)]^2 \quad (1)$$

$$SSIM(x,y) = \frac{(2\mu_x\mu_y+c_1)(2\sigma_{xy}+c_2)}{(\mu_x^2+\mu_y^2+c_1)(\sigma_x^2+\sigma_y^2+c_2)} \quad (2)$$

MSE checks difference of every two relative pixels in two images. It squares these differences, sums them up and divides the sum of squares by the total number of pixels in the images. An MSE of value 0 indicates that two pictures are perfectly identical. The greater the value of MSE is, the more errors rendered pictures create. However, MSE simply compares the distance between pixel intensities. There is a need to compare the structural information of images. The SSIM method can perceive changes in small sub-samples, whereas MSE estimates the perceived errors in the entire images. In equation two, (x,y) indicates the $N \times N$ sub-window in each image, and SSIM can be calculated on various windows of an image. The SSIM value can range between -1 and 1, where 1 represents perfect identicality.

3 Case Study

IRT for energy audits usually has a requirement for a minimum indoor and outdoor temperature difference. The required temperature difference between indoor and outdoor for energy audits using IRT should be at least 10 °C (18 °F)[12]. In order to meet this requirement, we conducted our case study on a university campus in Boston, USA. According to the *105 CMR 410.00: Minimum Standards of Fitness for Human Habitation* published by Massachusetts Department of Public Health [13], regulation requires indoor temperatures of at least 64 °F at night and 68 °F during the day from September 15th to June 15th. During the data acquisition for our case study in Boston the outdoor temperature was 30.2 °F at 7:00 AM and 43 °F at 10:00 AM when we conducted the research.

In this case study, we tested 3 different factors, flight patterns, camera angles, and overlap of images. Due to the complexity of this study, we tested vertical grid (parallel to north-south direction), horizontal grid (parallel to east-west direction) and their combination mesh grid in the area for flight patterns factor, 90 degrees (facing the ground) and 45 degrees (to the horizon) for camera angle factor, and 90% and 85% for the overlap of images. Table 2 shows the 8 flight configurations that were implemented in this study

In table 2, Number of calibrated images indicates how many images were calibrated to create 3D mapping. The pictures which were not calibrated and did not match with other images did not contribute to the creation of 3D points and meshes. 2D key points features were extracted from images by using SIFT or SURF as was explained in the research method above. 3D points were matched to 2D key points and indeed contributed to the creation of 3D models. The reprojection error referring to the image distance between a projected point and a measured one was introduced to quantify how closely an estimate of a 3D point recreates the point's true projection.[14]

Table 2. Summary of different flight configuration

| Session	Flight Pattern	Camera Angle	Front Overlap	Side Overlap	Number of Calibrated Images	Number of 2D Key points Observations for Bundle Block Adjustment	Number of 3D Points for Bundle Block Adjustment	Mean Reprojection Error [pixels]	Abbreviation
1	Horizontal Grid	45	90	65	505 out of 512 images calibrated (98%)	418410	121473	0.208	45-h
2	Vertical Grid	45	90	65	590 out of 592 images calibrated (99%)	490601	142500	0.209	45-v
3	Complete Mesh Grid	45	90	65	1099 out of 1104 (99%)	935059	274080	0.198	45-com
4	Complete Mesh Grid	45	85	65	884 out of 887 images calibrated (99%)	734397	224810	0.191	45-com-85
5	Horizontal Grid	90	90	65	539 out of 651 images calibrated (82%)	237600	77236	0.205	90-h
6	Vertical Grid	90	90	65	560 out of 644 images calibrated (86%)	214038	70300	0.216	90-v
7	Complete Mesh Grid	90	90	65	946 out of 1295 images calibrated (73%)	371617	123600	0.207	90-com
8	Complete Mesh Grid	90	85	65	720 out of 1040 images calibrated (69%)	263227	90663	0.195	90-com-85

4 Result and Discussion

Two cases for comparison were created for each flying session as demonstrated on Table 2. One was facing doors and windows and the images were captured by a camera from a fixed location on the ground as shown in Figure 4 (a). The left image was a rendered image, and the right one was a camera captured image. Therefore, there was only one scenario for doors and windows.

For the other case the flight acquired data facing the roof with 90 degrees and 45 degrees camera angles. The camera captured images were direct bird view images. Two 3D models were reconstructed with all 90-degree images and all 45-degree images, each of those two models produced four rendered images two with 90-degrees and two with 45-degrees by the use of model based virtual cameras. The two 90-degree rendered images from models were compared to a 90-degree camera captured image and the same was done for the 45-degree rendered images from models. Due to the camera angle, the visual perception of the camera captured images was totally different between 90 degrees and 45 degrees. This was also the reason for the cross comparison of both scenarios. The images shown in Figure 4, (b) is for 45 degrees camera, while (c) is for 90 degrees camera. The left ones are rendered images and the right ones are camera captured pictures in both (b) and (c). The rendered images in (b) and (c) are both from a model reconstructed from all 45-degree im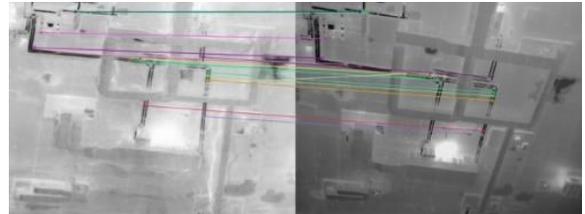ages. A comparison of two rendered images from a model reconstructed using all 90-degree images with two camera captured images were also conducted, but they are not shown here.
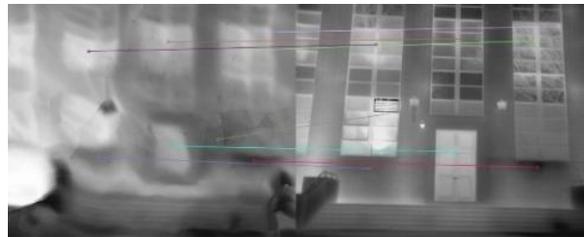
(a) Comparison of façade case
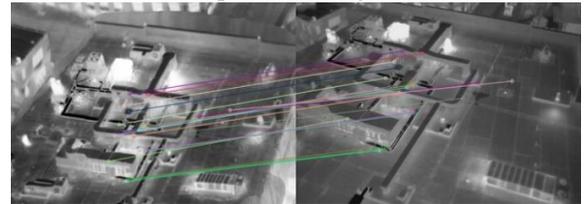
(b) Comparison of roof systemcase – 45-degree scenario

(c) Comparison of roof systemcase – 90-degree scenario

Figure 4. Illustration of match points between
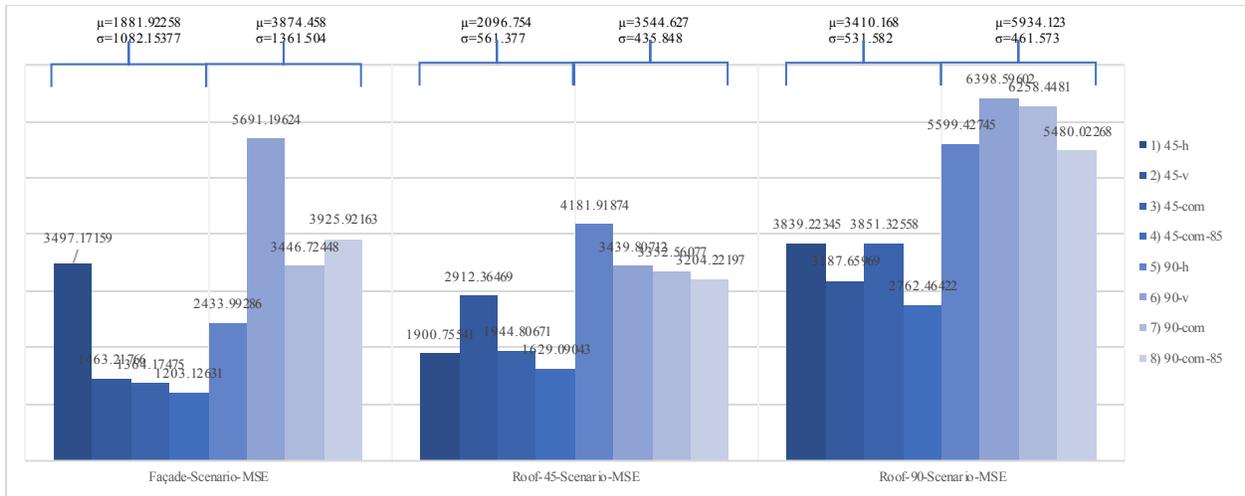
camera captured pictures and rendered pictures

In Figure 4, the solid lines illustrate the match points between rendered images and captured images. Match points, MSE, and SSIM were calculated and plotted in Figure 5. The legend in Figure 5 refer to the *abbreviations* on table 2. Average and standard deviation of flying session 1-4 and flying session 5-8 in different comparisons are calculated and shown on the top bar charts. According to Figure 5 (a), two roof system scenarios created more numbers of match points than door and windows scenario. As for those two roof system scenarios, a model reconstructed by a flight camera angle of 45 degrees can create more numbers of match points in its rendered images than a model generated by a flight camera angle of 90 degrees can in both scenarios. Average numbers of match points in 90-degree and 45-degree rendered images from a model with a flight camera angle of 45 degrees (session 1-4) are 958.250 and 1055.250 calculated based on the captured images taken by a 90-degree camera and on a 45-degree camera respectively, while those numbers are 547.500 and 706.500 in rendered images from a model with a flight camera angle of 90 degrees (session 5-8). More match points indicate that rendered images have a better performance in terms of capturing control points. To test

color rendering performance and structure similarity performance, MSE and SSIM are introduced in Figure 5 (b) and (c). According to Figure 5 (b), rendering images from a model with a 90-degree flight camera angle (session 5-8) performed worse than rendering images from a model with a 45-degree flight camera angle (session 1-4) in all scenarios in terms of capturing color information, because they had higher MSE scores. In Figure 5 (b), the session *"45-h"* where the flight camera angle was 45 degree, and the flight pattern was horizontal obtained a rendering image in façade scenario whose MSE was 3497.17159. This abnormal score is bigger than the average score plus standard deviation which should be considered an outlier. In Figure 5 (c), rendered images from a model reconstructed by all images with a 90-degree flight camera angle performed better than rendered images from a model with a 45-degree flight camera angle in both two roof system scenarios because of the higher SSIM scores. However, it was entirely different in scope for façade scenarios. Rendering images from a model with a 45-degree flight camera angle obtained 0.641 for average score of all flight patterns, which is higher than 0.593 average score obtained by rendering images from a model with a 90-degree flight camera angle.
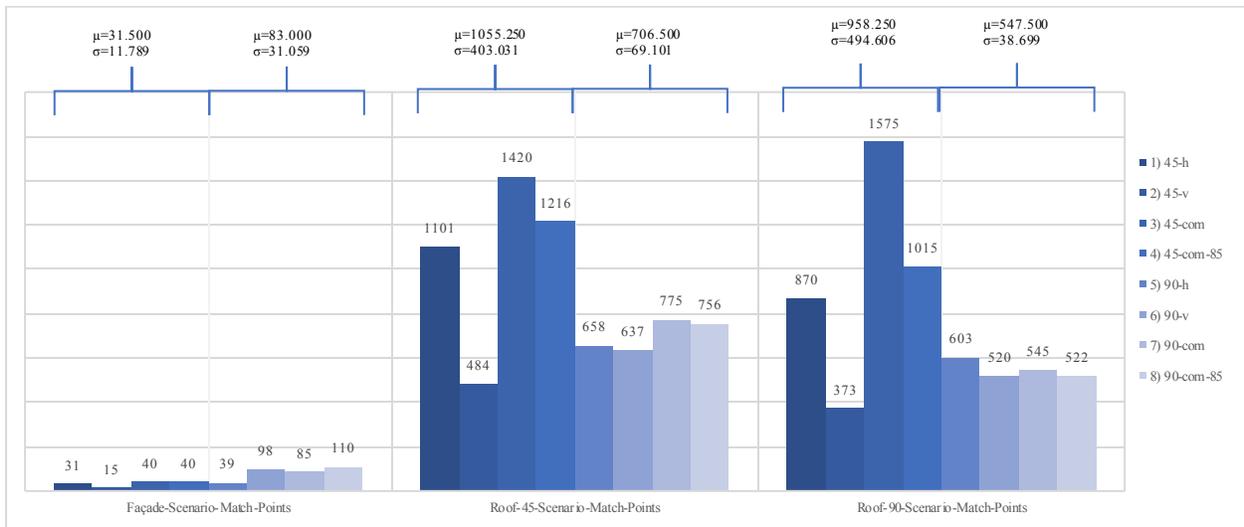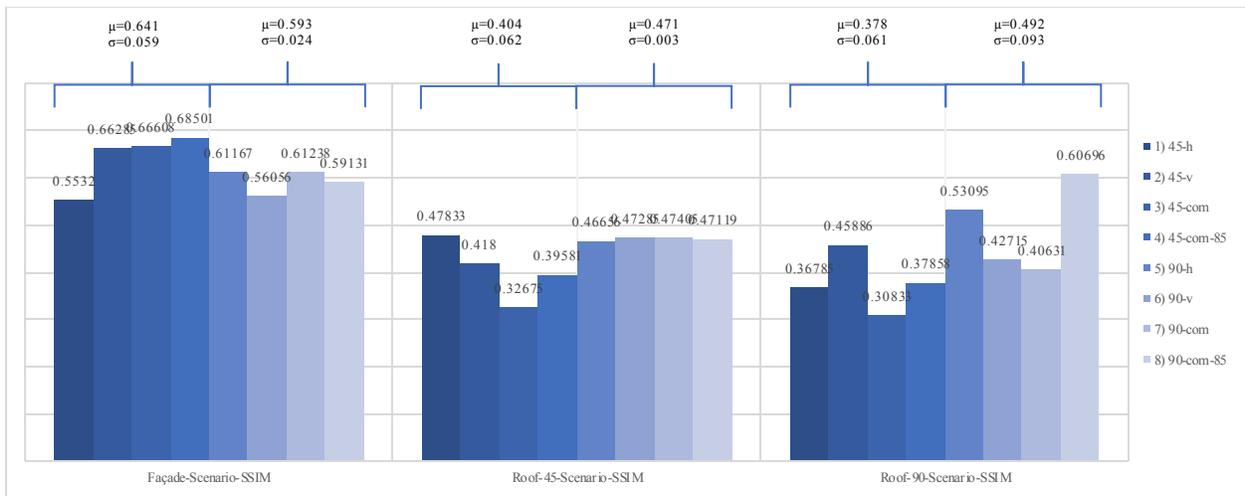

(a) Key points

Figure 5. Statistics of match points, MSE, and SSIM for different flying configurations

(b) MSE

μ=1881.92258 σ=1082.15377 | μ=3874.458 σ=1361.504 | μ=2096.754 σ=561.377 | μ=3544.627 σ=435.848 | μ=3410.168 σ=531.582 | μ=5934.123 σ=461.573

Façade-Scenario-MSE: 3497.17159, 1163.21766, 1369.17475, 1203.12631, 5691.19624, 2433.99286, 3446.72448, 3925.92163

Roof-45-Scenario-MSE: 1900.75551, 2912.36469, 1944.80671, 1629.09043, 4181.91874, 3439.80712, 3532.56077, 3204.22197

Roof-90-Scenario-MSE: 3839.22345, 3851.32558, 3387.65999, 2762.46422, 5599.42745, 6398.59602, 6258.4481, 5480.02268

Legend:
1) 45-h
2) 45-v
3) 45-com
4) 45-com-85
5) 90-h
6) 90-v
7) 90-com
8) 90-com-85

(c) SSIM

μ=0.641 σ=0.059 | μ=0.593 σ=0.024 | μ=0.404 σ=0.062 | μ=0.471 σ=0.003 | μ=0.378 σ=0.061 | μ=0.492 σ=0.093

Façade-Scenario-SSIM: 0.5532, 0.66285, 0.66608, 0.68501, 0.61167, 0.56056, 0.61238, 0.59131

Roof-45-Scenario-SSIM: 0.47833, 0.418, 0.32675, 0.39581, 0.46658, 0.47285, 0.47406, 0.47119

Roof-90-Scenario-SSIM: 0.36787, 0.45886, 0.30835, 0.37858, 0.53095, 0.42715, 0.40631, 0.60696

Legend:
1) 45-h
2) 45-v
3) 45-com
4) 45-com-85
5) 90-h
6) 90-v
7) 90-com
8) 90-com-85

Figure 5. Statistics of match points, MSE, and SSIM for different flying configurations (continued)

Not only can flight angles have an influence on the performance, but also the flight patterns and the image overlaps. According to Figure 5 (b) and (c), mesh grid flight patterns can result in lower MSE and higher SSIM than a monotonous grid which can only have vertical or horizontal lines. However, as for the image overlaps, in this study, higher image overlaps (90 %) not always performed better than lower image overlaps (85%). More thermal images do not contribute to a better reconstruction of a 3D thermal model. Some thermal images cannot be calibrated and matched to each other. Observation in Figure 6 also confirmed this statement. There are holes on the roof system in a point cloud model no matter how much the images overlap. Different types of roof systems have different influences on performance. As the pix4D software manual mentioned, water surfaces, snow, and sand have almost no or little visual content due to its large uniform areas. Roofs of buildings may have versatile color in RGB images but may have monotonous thermal values, which means the color of roofs will be monotonous in thermal images. Those large uniform areas can result in a sparse point cloud model. Shown in Figure 6, there was some equipment on the left roof in Figure 6 (a). Thus, sufficient points could be created. However, less points could be created on the right roof in Figure 6 (a). Figure 6 (b) is a mesh model fitted from a point cloud model.
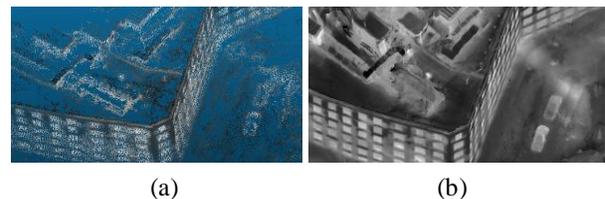
(a) (b)

Figure 6. Thermal point cloud model and mesh model

5 Conclusions

UAS has been introduced into a great number of research fields. It also has been utilized to capture energy loss from a single building. However, to audit energy loss from a group of buildings in a district and to create a 3D thermal model for infrastructure use are still challenges in terms of the efficiency and performance. Methodologically, different drone flying configurations in terms of flight patterns (vertical grid, horizontal grid and mesh grid), camera angles (90 and 45 degrees), and the percentage of image overlap (90% and 85%) were tested over a group of buildings in a district in this study.

Empirically, a flight camera angle of 90 degrees could capture more details on the roof system, whereas a flight camera angle of 45 degrees is more suitable for capturing details on façades. Also, more images could obtain a perfect 3D model. According to the result in this study, A flight angle of 90 degrees does exceed a flight angle of 45 degrees on roof case, and a flight angle of 45 degrees outperform a flight angle of 90 degrees on façade case in terms of structure similarity performance. As for color rendering, a flight angle of 90 degrees has a disappointing performance in both roof and façade cases. Indeed, mesh flight patterns are suggested over single grid patterns. As for the overlap of images, more thermal images might introduce more outliers. The algorithms can have difficulties in reconstruction. Additionally, no matter how many images are utilized, it is hard to create a 3D thermal model for a flat roof system which has large uniform areas. If both RGB and thermal images can be captured from the same angles and altitude, a detailed 3D model can be created by high resolution RGB images, and thermal textures can then be projected on top of the 3D model. This is the next factor's influence on efficiency and performance 3D Thermal Mapping we plan to explore.

Reference

[1] O. Friman *et al.*, "Methods for Large-Scale Monitoring of District Heating Systems Using Airborne Thermography Methods for Large-Scale Monitoring of District Heating Systems using Airborne Thermography," vol. 52, no. 52, pp. 5175–5182, 2014.

[2] S. Zhou, Z. O'Neill, and C. O'Neill, "A review of leakage detection methods for district heating networks," *Appl. Therm. Eng.*, vol. 137, no. April, pp. 567–574, 2018.

[3] P. A. Fokaides and S. A. Kalogirou, "Application of infrared thermography for the determination of the overall heat transfer coefficient (U-Value) in building envelopes," *Appl. Energy*, vol. 88, no. 12, pp. 4358–4365, 2011.

[4] E. Barreira, R. M. S. F. Almeida, and J. M. P. Q. Delgado, "Infrared thermography for assessing moisture related phenomena in building components," *Constr. Build. Mater.*, vol. 110, pp. 251–269, 2016.

[5] E. Lucchi, "Applications of the infrared thermography in the energy audit of buildings: A review," *Renew. Sustain. Energy Rev.*, vol. 82, no. May 2017, pp. 3077–3090, 2018.

[6] T. Rakha and A. Gorodetsky, "Review of Unmanned Aerial System (UAS) applications in the built environment: Towards automated building inspection procedures using drones," *Autom. Constr.*, vol. 93, no. January, pp. 252–264, 2018.

[7] A. Kylili, P. A. Fokaides, P. Christou, and S. A. Kalogirou, "Infrared thermography (IRT) applications for building diagnostics: A review," *Appl. Energy*, vol. 134, pp. 531–549, 2014.

[8] E. Lucchi, "Applications of the infrared thermography in the energy audit of buildings: A review," *Renew. Sustain. Energy Rev.*, vol. 82, no. November 2017, pp. 3077–3090, 2018.

[9] M. Fox, S. Goodhew, and P. De Wilde, "Building defect detection: External versus internal thermography," *Build. Environ.*, vol. 105, pp. 317–331, 2016.

[10] R. Bai, J. Zhao, D. Li, and W. Meng, "A new technique of camera calibration based on X-target," *Commun. Comput. Inf. Sci.*, vol. 97 CCIS, no. PART 1, pp. 39–46, 2010.

[11] J. L. Schonberger and J.-M. Frahm, "Structure-From-Motion Revisited," *IEEE Conf. Comput. Vis. Pattern Recognit.*, 2016.

[12] FLIR Systems, "An informative guide for the use of thermal imaging cameras for inspecting buildings, solar panels and windmills. THERMAL IMAGING GUIDEBOOK FOR BUILDING AND RENEwABLE ENERGy APPLICATIONS Content," *Guid B.*, p. 68, 2011.

[13] Massachusetts Department of Public Health, "105 CMR 410.000: Minimum Standards of Fitness for Human Habitation (State Sanitary Code, Chapter II)," *J. Exp. Psychol. Gen.*, vol. 136, no. 1, pp. 23–42, 2007.

[14] H. Richard and A. Zisserman, *Multiple View Geometry in computer vision*. Cambridge University Press, 2003.